CHAPTER 115

BED SHEAR STRESS AND SCOUR AROUND COASTAL STRUCTURES

B.M. Sumer[1], J. Fredsøe[1], N. Christiansen[1] and S.B. Hansen[1]

Abstract

Two kinds of experiments were made: 1) Rigid-bed experiments and 2) erodible-bed experiments. In the former experiments, bed shear stresses were measured around three kinds of structures: 1) a vertical circular cylinder, 2) a cone-shaped structure and 3) the head of a breakwater (with and without side slopes). The results are presented in terms of amplification in the bed shear stress for the structures considered.

In the erodible-bed experiments, actual scour tests were carried out with the aforementioned structures. The results regarding the scour tests are related to the measured bed shear stress.

1. Introduction

Considerable knowledge may be gained on scour around coastal structures by studying the bed shear stress on the unscoured bed, one of the hydrodynamic quantities directly related to scour.

The purpose of the present study is to investigate the bed shear stress around three kinds of coastal structures, namely a vertical pile, a cone-shaped structure and a breakwater, and to relate it to the resulting scour. The cone-shaped structure has been selected, to study the effect of side slopes on the complex vortex system responsible for scour around the structures. As regards the breakwater structure, attention is concentrated on the three-dimensional scour around the head of the breakwater.

[1] Institute of Hydrodynamics and Hydraulic Engineering (ISVA), Technical University of Denmark, 2800 Lyngby

2. Experiments

2.1. Bed-shear stress measurements

The experiments were conducted in a flume facility the size of 26.5 x 0.6 x 0.8 m. In most of the cases, the model structures were exposed to both waves and steady currents.

A two-component hot-film probe (DANTEC 55R46 spec.) was used in the experiments. The probe was flush-mounted with the rigid bed of the flume. It enabled the magnitude and the heading of the bed shear stress vector to be measured. The details about the probe and the other pertinent information have been reported elsewhere (Sumer et al., 1993).

Three kinds of structures were implemented in the tests (Fig. 1): 1) A vertical cylinder with a circular cross section (one with diameter D = 4 cm and the other with D = 9 cm), 2) a cone-shaped structure (one with β = 45° side slope and the other with β = 30° side slope; both with the same base diameter, namely D = 9 cm), and finally 3) a breakwater with and without side slopes. In the case of the breakwater with side slopes, simulating a rubble-mound breakwater, the angle of the side slopes was 45°. The relatively high value of the side slope was due to experimental constraints. The base width of the breakwater was B = 3 cm in the vertical wall breakwater case and B = 11.5 cm in the rubble-mound case.

The bed shear stress measurements were supported in a few cases with velocity measurements where a one-component DANTEC Laser Doppler Anemometer was used.

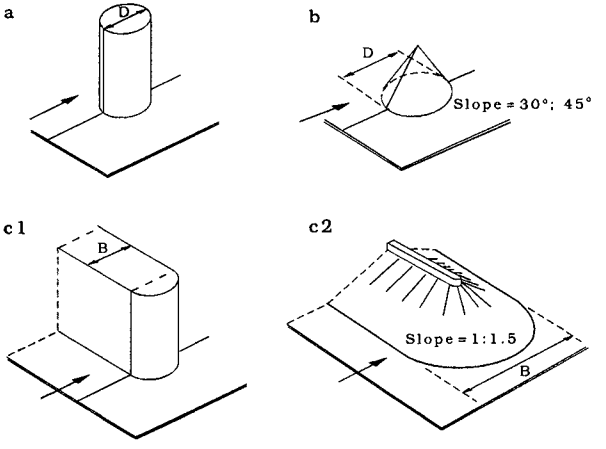

Fig. 1 Structures considered in the present study. a: Vertical cylinder. b: Cone (β = 30° and 45°). C1: Vertical-wall breakwater. C2: Rubble-mound breakwater (side slope = 1:1 in the bed shear stress meas. and 1:1.5 in the scour expts.).

TABLE 1. Test conditions

Structures	Sand size, d_{50} (mm)	Diameter of cylinder and cone, D or base width of breakwater, B (mm)	Water depth, h (cm)	Wave period, T (s)	Flow velocity V or U_m (cm/s)	Friction velocity U_f or U_{fm} (cm/s)	Shields parameter θ	Keulegan-Carpenter number KC	Structure Reynolds number Re	Remarks
Vertical circular cylinder	0.18-0.36	10-200	40	1.2-4.5	11-53	1.3-3.3	0.04-0.4	5-∞	3×10^3-1×10^5	Reported in Sumer et al. (1992)
"	0.44	510	3-6.5	-	30-34	2.1	0.06	∞(steady c.)	2×10^5	
Cone with side slope β = 30°	0.16	860	53	-	33	1.6	0.1	"	3×10^5	
"	"	"	43	2.5	36	2.5	0.25	1	"	
Cone with side slope β = 45°	"	880	53	-	33	1.6	0.1	∞(steady c.)	"	
"	"	"	50	2.5	34	2.4	0.2	1	"	
Head of vertical-wall breakwater	0.17	140-400	40	1.5-4	11-45	1.3-2.6	0.06-0.25	0.5-10	2×10^4-1×10^5	Reported in Gökçe et al. (1994)
Head of rubble-mound breakwater with side slope 1:1.5	"	2400	"	4.9	20	1.2	0.05	0.4	5×10^5	

2.2. Scour experiments

The scour processes around the structures were videotaped, using an underwater mini video camera in most of the cases. These experiments were carried out in three facilities, namely in a small scale flume (the same as that used in the bed shear stress measurements) and in two medium scale flumes (one with dimensions 28 x 4 x 1 m and the other 23 x 2 x 0.5 m).

In all the wave tests, the orbital velocity of the undisturbed flow at the bottom was measured. In the current tests, the undisturbed velocity profile over the depth was measured. Similar to the bed shear-stress measurements, three kinds of structures were used in the scour experiments: 1) Vertical circular cylinders, 2) cone-shaped structures and 3) breakwaters. Table 1 summarizes the test conditions of the scour experiments.

In the table, V is the mean flow velocity in the case of steady current and U_m is the amplitude of the orbital velocity at the bed in the case of waves, while U_f and U_{fm} are the corresponding friction velocities in the case of steady current and in the case of waves, respectively. θ is the Shields parameter defined by

$$\theta = \frac{U_f^2}{g(s-1)d} \tag{1}$$

in which g is the acceleration due to gravity and s is the relative density of sand grains. U_f is replaced by U_{fm} in the case of waves. In the table, KC, the Keulegan-Carpenter number, is defined by

$$KC = \frac{U_m T}{D} \quad or \quad KC = \frac{U_m T}{B} \tag{2}$$

and Re, the Reynolds number,

$$Re = \frac{U_m D}{\nu} \quad or \quad Re = \frac{U_m B}{\nu} \tag{3}$$

From the table, it is seen that all the scour experiments were conducted under live-bed conditions, $\theta > \theta_{cr}$, in which θ_{cr} is the critical value of θ corresponding to the initiation of motion on the sand bed.

3. Results and discussion

3.1 Bed shear stress

Cylinder

The bed shear stress around a vertical cylinder placed on

a plane bed is increased due to the following three effects: 1) the contraction of streamlines near the structure 2) the horse-shoe vortex and 3) the vortex shedding (Fig. 2).

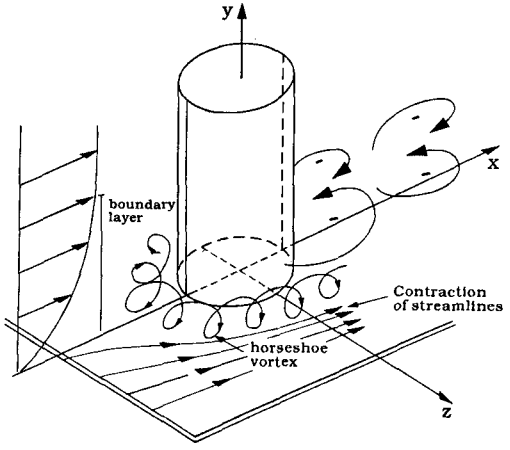

Fig. 2 Definition sketch. Near-bed flow structures around a vertical cylinder.

The mechanisms related to these effects and their role in the scour processes have been discussed in Breusers et al. (1977), Hjorth (1975), Baker (1979), Dargahi (1987) in steady current and Sumer et al. (1992) in waves.

Fig. 3 illustrates the distribution of the bed shear stress along the principal axes x and z in the case of *steady current*. In the figure, α is the amplification in the bed shear stress

$$\alpha = \frac{\tau_0}{\tau_{0\infty}} \tag{4}$$

in which τ_0 is the bed shear stress and $\tau_{0\infty}$ is that corresponding to the undisturbed flow. The figure includes also the results of Baker (1979) who obtained the bed shear stresses from the measured velocity profiles. (It is seen that the present results and the results of Baker agree fairly well despite the differences in the test conditions and in the flow environment). While Fig. 3b illustrates the amplification in τ_0 near the side edges of the cylinder due to contraction ofthe flow, Fig. 3a shows the amplification in τ_0 both in front of the cylinder (beneath the horse-shoe vortex) and at the rear side of the cylinder (in the lee-wake region).

It is seen that the increase in the bed shear stress near the cylinder can be as much as by a factor 10 or even larger. Similar results were obtained also by Hjorth (1975) (Fig. 4a).

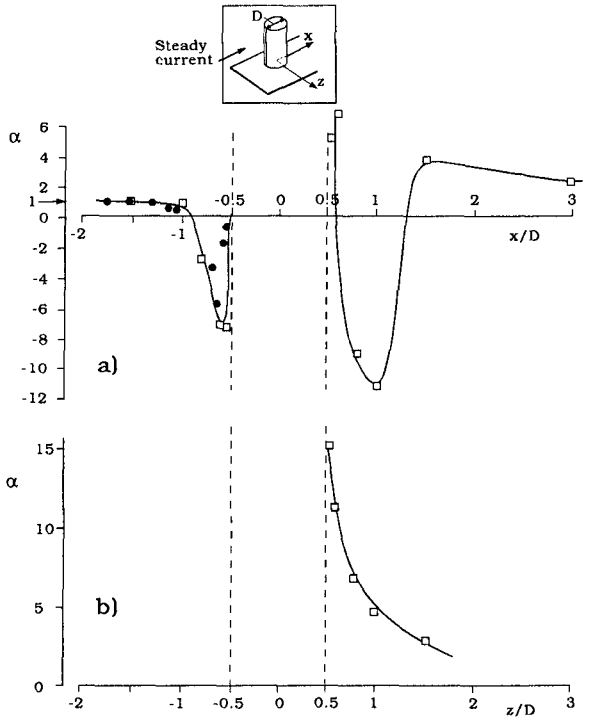

Fig. 3 Amplification in the shear stress along the principal axes x and z around a vertical cylinder. Squares: Present experiments (flow-depth, h = 40 cm, D = 9 cm and V = 8.7 cm/s and Re = 7800). Circles: Baker's (1979) experiments in air (D = 7.6 cm, V = 51 cm/s, $D/\delta^* = 14.8$ and Re = 2610, δ^* being the displacement thickness of the boundary layer on the bottom).

Fig. 4 compares the distribution of the bed shear stress near the cylinder in the case of steady current (Hjorth, 1975) with that measured in the present study in the case of waves (where KC, the Keulegan-Carpenter number, is 10) while Fig. 5 gives a 3D illustration of the latter flow, at the phase value $\omega t = 0$, corresponding to the passage of the wave crest. In Fig. 4, α is the amplification in the bed shear stress defined by

$$\alpha = \frac{|\vec{\tau}_0|}{\tau_{0\infty}} \quad ; \quad \textit{steady-current case} \tag{5}$$

and

$$\alpha = \frac{Max|\vec{\tau}_0|}{\tau_{0m}} \quad ; \quad \textit{wave case} \tag{6}$$

in which τ_{0m} is the maximum value of the bed shear stress corresponding to the undisturbed flow.

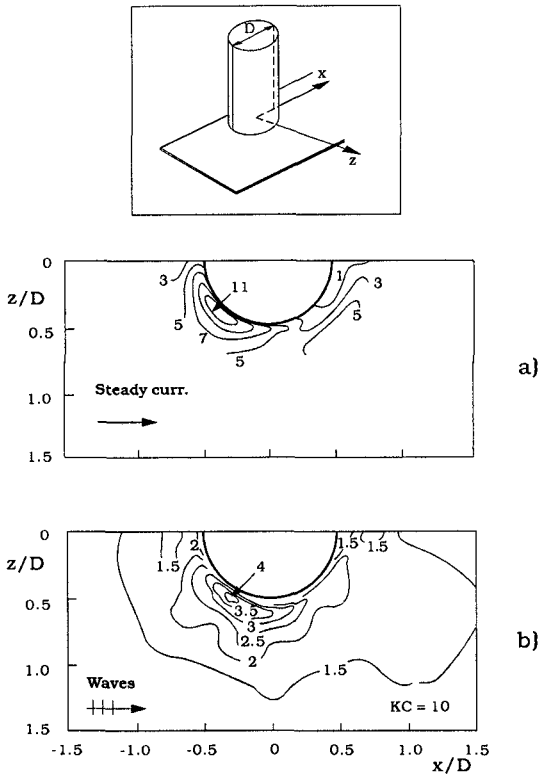

Fig. 4 Amplification in the bed shear stress. a: Steady current (D = 7.5 cm, V = 30 cm/s, h = 20 cm) (from Hjorth (1975)). b: Waves (D = 4 cm, U_m = 9.2 cm/s, T = 4.4 s, h = 40 cm).

Fig. 4 indicates that, in the case of waves, the amplification factor is not as large as in steady currents; the increase in the bed shear stress with respect to its undisturbed value is only a factor 3-4 in the best condition. Measurements show that this is the case also for other KC numbers (up to KC = 100), see Sumer et al. (1992). Fig. 6 depicts the distribution of amplification along the principal axes x and z. It seems that the measurements as regards the z-variation of α apparently agree quite well with the potential-flow prediction (Fig. 6b).

As seen from Fig. 4, there is a factor 3 difference between the amplification in steady currents and that in waves. This may be attributed to the rather thin boundary layer developing

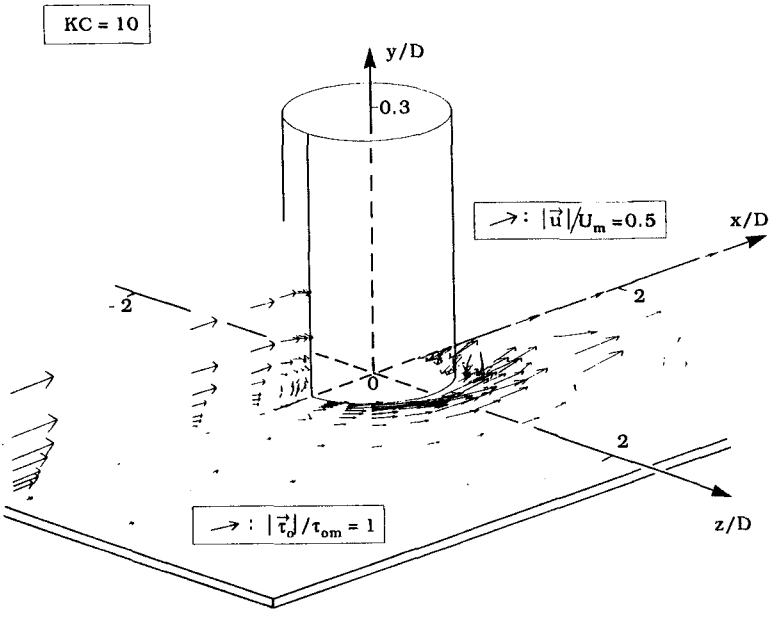

Fig. 5 Three-dimensional vector-diagram illustration of near-bed flow around a vertical circular cylinder at the phase value $\omega t = 90°$, i.e. at the time of crest passing (D = 4 cm, U_m = 9.2 cm/s, T = 4.4 s, h = 40 cm).

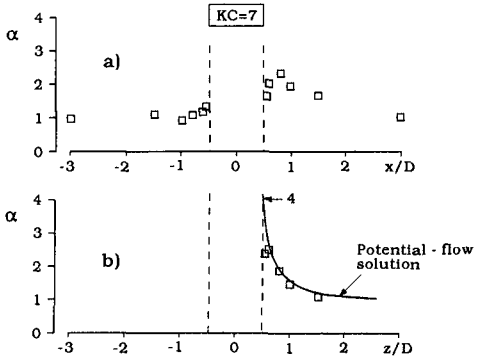

Fig. 6 Amplification in the bed shear stress around a vertical circular cylinder along the principal axes x and z (D = 9 cm, U_m = 31.8 cm/s, T = 1.9 s, h = 40 cm).

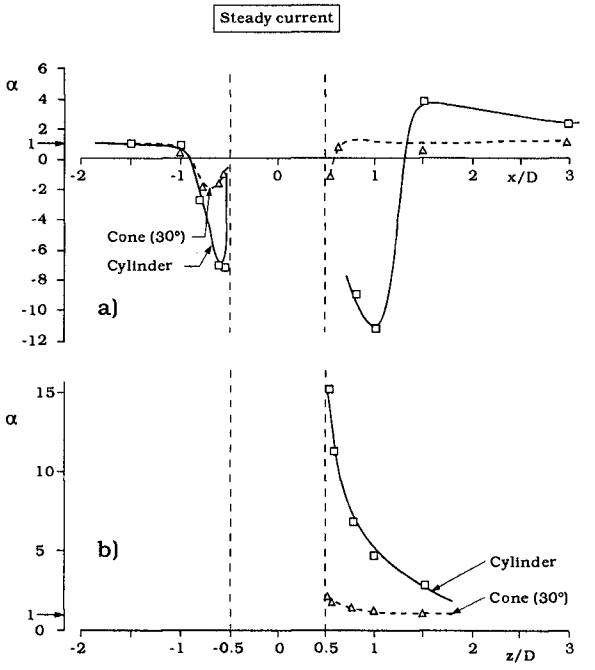

Fig. 7 Comparison of the bed-shear stress amplification around the cylinder and the cone. (Test conditions are the same as in Fig. 3 for the cylinder test. For the cone test: D = 9 cm, V = 8.7 cm/s, h = 40 cm).

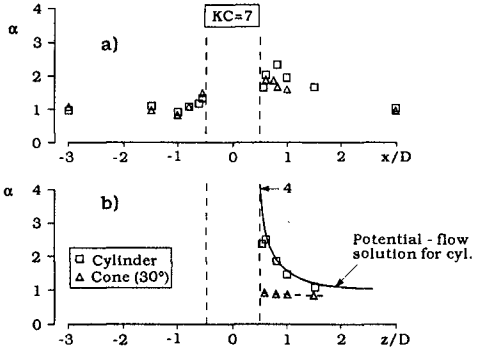

Fig. 8 Comparison of the bed-shear stress amplification around the cylinder and the cone. (Test conditions are the same as in Fig. 6 for the cylinder test. For the cone test: D = 9 cm, U_m = 31.8 cm/s, T = 1.9 s, h = 40 cm).

over the bed in the case of waves. The previously mentioned agreement between the measurements and the potential-flow prediction substantiates the latter argument. In the case of steady current, however, the combined action of the horse-shoe vortex and the contraction of flow near the side edges of the cylinder amplifies the bed shear stress tremendously, to give an α value of O(10) (Figs. 3b and 4a). The strong presence of horse-shoe vortex in the steady-current situation accounts for also the large increase in the bed shear stress in front of the cylinder (Fig. 3a).

Cone

Figs. 7 and 8 compare the cone results with the cylinder results along the principal axes x and z. It is clear that the net effect of side slopes (the cone case) is to decrease the bed shear stress. From the preceding figures, the following conclusions may be drawn.

1) Fig. 7a shows that τ_0 decreases by a factor of about 4 underneath the *horse-shoe vortex* (in the area extending over $-1 \leq x/D \leq -0.5$) in the case of cone. (It is interesting to note that the horse-shoe vortex is still existent in the cone case, but its strength is greatly reduced with respect to the cylinder situation).

The decrease in τ_0 is due to the large decrease in the adverse pressure gradient which builds up at the upstream side of the structure and is known to be responsible for the formation of horse-shoe vortex. This decrease in the adverse pressure gradient is simply because of the favourable cone geometry.

It may be noticed that the cone and the cylinder results are almost identical in the case of waves at the upstream side of the structure (Fig. 8a). This is simply because no horse-shoe vortex exists for this KC number, not even in the case of cylinder (Sumer et al. (1992)). So, the results will obviously be the same. The 45°-cone experiments exhibited the same behaviour.

The results in Fig. 8a are not symmetric with respect to $x = 0$ due to the asymmetry in waves.

2) τ_0 decreases considerably also near the *side edges of the structure* in the case of cone; this decrease is about a factor 10 in the steady-current situation (Fig. 7b), while it is a factor 2-3 in the case of waves (Fig. 8b). Two effects are responsible for this large decrease in τ_0: 1) the contraction of streamlines near the side edges of the cone structure is rather small; and also, 2) the horse shoe vortex is rather weak in this case, as mentioned above.

3) Similar observations can be made also in *the lee-wake* area. Tremendous decrease (by an order of magnitude) takes place in τ_0 in this area ($x \geq 0.5$) in the case of steady current (Fig. 7a), while practically no change takes place in the case of waves (Fig. 8a). This reduction in the bed shear stress

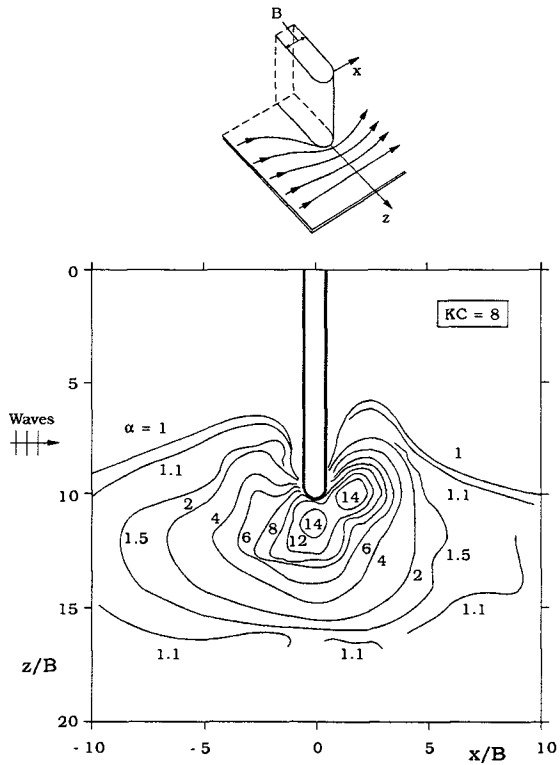

Fig. 9 Amplification in the bed shear stress around the head of a vertical-wall break-water. (B = 3 cm, U_m = 12 cm/s, T = 1.3 s, h = 40 cm).

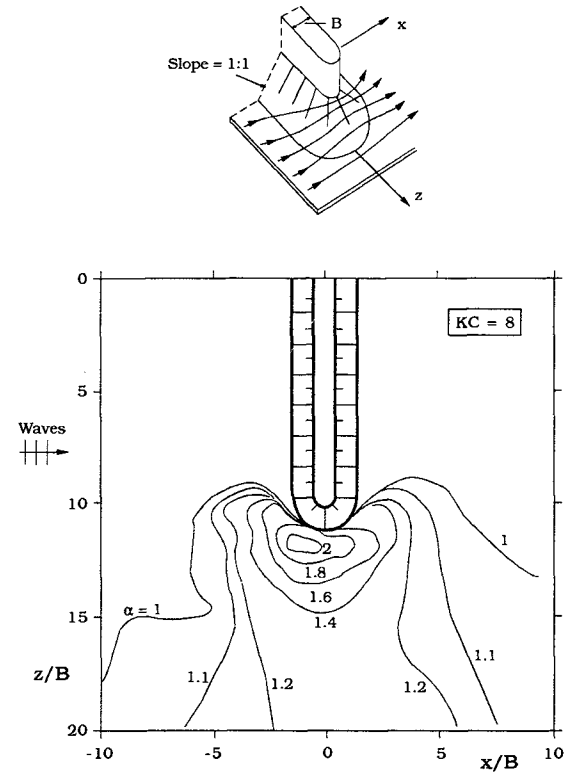

Fig. 10 Amplification in the bed shear stress around the head of a breakwater with side slopes. (B' ≅ 11.5 cm, U_m = 12 cm/s, T = 1.3 s, h = 40 cm).

is obviously related to the rather weak occurrence of vortex shedding in the case of cone.

Breakwater

Fig. 9 depicts the contour plot of the bed-shear-stress amplification, α, in the case of vertical-wall breakwater for KC = 8. As seen, the α values can be as high as 14 near the head of the breakwater. Similar behaviour was obtained for KC = 1 where a value of about 10 was measured for the maximum value of α.

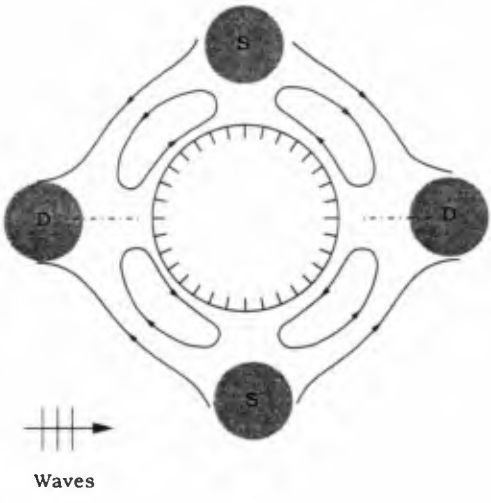

Fig. 11 Sketch illustrating the steady streaming around a large cylinder in waves. S: Scour. D: Deposition.

In a previous study undertaken at ISVA (Gökçe et al., 1994), the flow around the head of a vertical-wall breakwater was found to occur in the following three regimes: 1) Unseparated-flow regime when KC < 1, 2) separated-flow regime when 1 < KC $\lesssim$ 12 and 3) separated-flow regime with a horse-shoe type vortex in front of the breakwater when KC $\gtrsim$ 12.

Since the tested KC numbers, namely KC = 1 and 8, are well below the KC number beyond which the horse-shoe vortex emerges, no horse-shoe vortex was present in the present tests. This means that the only factor behind the extensive increase in τ_0 at the head of the breakwater is the effect of flow contraction including the one experienced during the flow reversal where the separation vortex is washed around the breakwater. This explains why α is a factor 3-4 larger in the present case (Fig. 9) than in the corresponding case of a circular cylinder (Fig. 4b) where the contraction effect is not as severe as in the case of breakwater.

Fig. 10 illustrates the effect of side slopes on the bed shear stress. The model used in the tests was exactly the same as that used in the vertical-wall breakwater tests (Fig. 9). The only difference is that the model was encircled with a sloping side wall on the bottom (as sketched in Fig. 10) with a slope 1:1. As seen, the effect is a large drop in the bed shear stress at the head of the breakwater. The maximum value of τ_0 is reduced by a factor 7 with respect to its value in the case of vertical-wall breakwater.

This large reduction is obviously related to the small flow contraction in the present case due to the geometry of the structure, similar to that when the structure is changed from a circular cylinder to a cone (Figs. 7b and 8b).

3.2 Scour

The scour data obtained in the case of cone (both with β = 30° and 45°) indicated that the smaller the side slope, the smaller the scour depth.

Secondly, it was apparent from the results that the scour depth in the case of cone (β = 30° and 45°) in steady current was one order of magnitude smaller than in the case of cylinder.

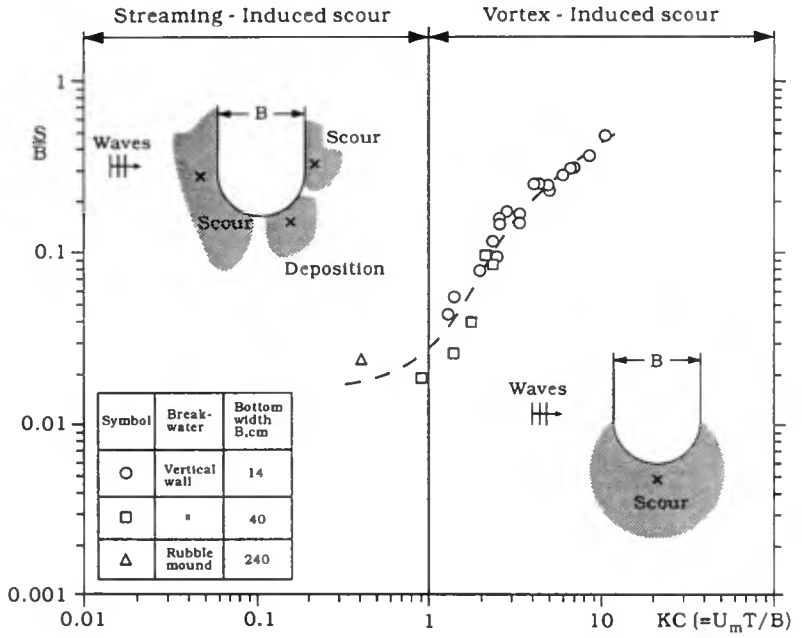

Fig. 12 Normalized scour depth at the head of breakwater as function of KC. For test conditions, see Table 1. ×: Maximum scour or deposition

Thirdly, the cone results corresponding to the wave case have been compared with the cylinder scour reported in Sumer et al. (1992). It was found that, for KC numbers above 5, the cone scour is on average below the cylinder scour. For very small KC numbers (KC = O(5)), however, the maximum scour depth appeared to be in the same order of magnitude as that measured in Sumer et al. (1992). This may be related to the not very extensive drop in the bed shear stress in the case of cone in waves (Fig. 8).

For extremely small KC numbers such as KC (1) (i.e., large structures), the scour is caused not by the vortex shedding but rather by various forms of steady streaming which build up around the structure. The steady streaming around a large cylinder is an example for this kind of streaming (Fig. 11). Here, the streaming is caused by the difference in the response of the cylinder boundary layer to the two successive half periods of the wave motion. This kind of steady streaming may cause a scour-and-deposition pattern around the structure, as sketched in Fig. 11.

The data related to the present breakwater-scour experiments are plotted in Fig. 12. As seen from the sketches in the figure, the scour hole occurring at the tip of the breakwater in the case of large KC-number situations disappears when KC becomes less than O(1). Instead, a streaming-induced scour-and-deposition pattern forms around the breakwater head, in the way as described in the preceding paragraph. The disappearance of the scour hole at the tip of the breakwater is due partly to the unseparated flow regime and partly to the large reduction in the bed shear stress (cf. Figs. 9 and 10).

The scale effects in connection with both the flow-description experiments and the scour tests have been discussed elsewhere (in Sumer et al. (1992 and 1993) in conjunction with scour around vertical piles and in Gökçe et al. (1994) in conjunction with scour around the head of a breakwater).

4. Conclusions

1) The bed shear stress around a vertical, circular cylinder is increased considerably (by a factor of 10) with respect to its undisturbed value when the cylinder is exposed to a steady current, while this increase is by a factor of 3-4 when it is exposed to waves.

2) For a cone-shaped structure, the increase in the bed shear stress near the structure is small, a factor of 2-4, regardless of the flow type (steady current or waves).

3) The increase in the bed shear stress around the head of a vertical-wall breakwater (which is exposed to waves) is a factor of 10 or so. When the breakwater is encircled at the bottom with a sloping side wall with a slope of 1:1, the increase in the bed shear stress is only a factor 2.

4) The scour depth around a cone-shaped structure is an order of magnitude smaller than in the case of cylinder struc-

ture in steady currents. In the case of waves, however, the scour depth appears to be smaller than that measured in the case of cylinder when KC > O(5). For KC = O(5), however, the cone scour is in the same order of magnitude as the cylinder scour.

5) Although the scour hole at the tip of the breakwater disappears in the case of rubble-mound breakwater (apparently due to the effect of the side slope), another mechanism, namely the steady streaming, may induce a scour-and-deposition pattern around the breakwater head.

Acknowledgement

This work was undertaken as part of MAST II "Monolithic (Vertical) Coastal Structures" and "Rubble Mound Breakwater Failure Modes" research programmes. It was funded jointly by the Danish Technical Research Council (STVF) under the programme "Marin Technique" and by the Commission of the European Communities, Directorate General for Science, Research and Development under MAST contracts No. MAS2-CT92-0042 and MAS2-CT92-0047.

Appendix. References

Baker, C.J. (1979). The laminar horseshoe vortex. J. Fluid Mech., Vol. 95, part 2, pp. 347-367.

Breusers, H.N.C., Nicollet, G. and Shen, H.W. (1977). Local scour around cylindrical piers. J. Hydr. Res., 15(3), pp. 211-252.

Dargahi, B. (1987). Flow field and local scouring around a cylinder. Hyd. Lab., the Royal Inst. of Technology, Stockholm, Sweden. Bulletin No. TRITA-VBI-137, iii + 230 p.

Gökçe, T., Sumer, B.M. and Fredsøe, J. (1994). Scour around the head of a vertical-wall breakwater. Proceedings of the International Conf. on Hydro-Technical Engrg. for Port and Harbour Construction, Yokosuka, Japan, 19-21 Oct.

Hjorth, P. (1975). Studies on the nature of local scour. Dept. of Water Resources Engineering, Lund Inst. of Tech-nology, Univ. of Lund, Sweden, Bulletin Series A, No. 46.

Sumer, B.M., Christiansen, N. and Fredsøe, J. (1993). Influence of cross section on wave scour around piles. ASCE, J. of Waterway, Port, Coastal and Ocean Engineering, Vol. 119, No. 5, Sept./Oct., pp. 477-495.

Sumer, B.M., Fredsøe, J. and Christiansen, N. (1992). Scour around vertical pile in waves. ASCE, J. of Waterway, Port, Coastal and Ocean Engineering, Vol. 118, No. 1, Jan./Feb., pp. 15-31.

Sumer, B.M., Arnskov, M.M., Christiansen, N. and Jørgensen, F.E. (1993). Two-component hot-film probe for measurements of wall shear stress. Experiments in Fluids, Vol. 15, pp. 380-384.